Highlights

A Novel Credibility Evaluation and Mitigation for Ranging Measurement in UWB Localization

Hongchao Yang, YunJia Wang, Chee Kiat Seow, Meng Sun, Wout Joseph, David Plets

- Credibility evaluation system for UWB ranging measurement;
- Fine-grained classification of ranging measurement errors and mitigation strategies based on credibility;
- The targeted models for correcting ranging measurement errors caused by different factors.

A Novel Credibility Evaluation and Mitigation for Ranging Measurement in UWB Localization

Hongchao Yang[a,b], YunJia Wang[b], Chee Kiat Seow[c], Meng Sun[b], Wout Joseph[d] and David Plets[d]

[a]Dalian Maritime University, LingHai Road, Dalian, 116026, China
[b]China University of Ming and Technology, Daxue Road, Xuzhou, 221116, China
[c]University of Glasgow, University Ave, Glasgow, G12 8QQ, U.K
[d]Ghent University, Zwijnaarde, Ghent, 9052, Belgium

ARTICLE INFO

Keywords:
UWB
CIR
Credibility Evaluation
Ranging Measurement Mitigation
Indoor Positioning
BERT

ABSTRACT

UWB ranging measurements are prone to positive bias errors in NLOS conditions. Existing algorithms often use a uniform model to correct various ranging measurement errors, which has poor performance and fails to fully utilize the advantages of UWB technology. This article proposes a credibility evaluation system for assessing the quality of ranging measurement and the error fine-grained classification. For different sources of ranging measurement errors, we develop optimization models that integrate BERT with LSTM, focusing on both temporal and energy information, and extending the correction range to LOS measurements. In multi-scenario experiments, the credibility evaluation error was 0.047, with LOS and NLOS ranging measurement errors reduced by 37.9% and 80.94%, respectively. This approach outperforms LS-SVM, CNN, and CNN-LSTM by 57.21%, 43.2%, and 18.99%. After optimization, centimeter-level positioning accuracy improved by 30.2%, and the average error was reduced by 69.68%, surpassing advanced algorithms by 42.53%, 43.61%, and 44.00%.

1. Introduction

Location-Based Service (LBS) is a crucial support for the future era of artificial intelligence. While mature and commercial Global Navigation Satellite Systems (GNSS) [1] provide stable outdoor location, their signals cannot penetrate buildings, rendering them ineffective for indoor location. Indoor positioning [2] technology requires additional sensors to provide accurate location, such as Wireless Fidelity (Wi-Fi) [3], Bluetooth (BLE) [4], Ultra-Wideband (UWB) [5], and Visible Light Positioning (VLP) [6]. Compared to other technologies, UWB [7] achieve higher precision ranging measurement through nanosecond narrow pulse signals, with a wide coverage range and advantages such as resistance to multipath interference and strong penetration, making it suitable for complex indoor environments. However, when the direct line-of-sight (LOS) between sensors is obstructed, resulting in a Non-Line-of-Sight (NLOS) condition, UWB may mistakenly identify the multipath signal following the true first path signal as the report first path signal. This results in positive bias errors in signal flight time and corresponding ranging measurements. Therefore, reducing NLOS ranging measurement error is crucial due to the increased frequency of NLOS phenomena caused by numerous obstacles and moving personnel in enclosed and complex indoor environments.

Existing UWB positioning algorithms initially perform channel identification, categorizing ranging measurements into high-precision LOS or low-precision NLOS. The LOS measurements are directly used for positioning, while the NLOS measurements, due to their significant errors, require correction before positioning to avoid reduced accuracy. Current NLOS ranging measurement error mitigation algorithms fall into two categories. The first methodology replace the NLOS ranging measurements with additional information from the same source UWB [8–10] or other positioning techniques [11–17]. The former requires increased UWB deployment density to ensure a higher proportion of LOS ranging measurements. The latter involves integrating additional positioning information such as Wi-Fi, BLE, or Inertial Measurement Units (IMU). This approach incurs high costs and system complexity, and the introduction of additional technologies limits the algorithm's application scenarios. The second method directly corrects NLOS ranging measurement errors by establishing a mapping relationship between inputs, such as channel characteristics, and ranging measurement errors [18, 19]. The Channel Impulse Response (CIR) sequence reflects the arrival time and energy attenuation of different path signals, which contains information corresponding to the actual ranging measurements. Deep learning methods [20], such as Convolutional Neural Networks (CNN) [21], Long Short-Term Memory (LSTM) [22] networks, and CNN-LSTM models [23], can self-learn relevant information from the original CIR sequence data to predict ranging measurement errors. Machine learning algorithms, such as Support Vector Machines (SVM) [24–26], can predict ranging measurement errors by combining artificial CIR features from the raw CIR sequence. However, existing algorithms cannot simultaneously account for CIR sequences related to timing information and CIR features related to energy information. Due to changes in environmental layout and the physical characteristics of obstacles, the impact of NLOS phenomena on ranging measurement accuracy varies. Existing algorithms that correct NLOS ranging measurement errors using a single model cannot

ORCID(s):

maximize accuracy. In theory, low-precision NLOS ranging measurements include high-precision results with minimal signal interference and high-error results with severe signal interference and low correction value. Additionally, current correction algorithms are limited to NLOS ranging measurements, which restricts their potential to improve positioning accuracy due to the limitations of channel recognition algorithms. To address these issues, this article proposes a fine-grained classification of NLOS ranging results based on the causes of ranging measurement errors and introduces a credibility evaluation model to enhance the advantages of UWB ranging measurement. By leveraging the deep bidirectional learning capability of the Transformer Bidirectional Encoder Representation (BERT) to balance the multidimensional input composed of time and energy features, various ranging measurement errors were optimized and extended to LOS results in a targeted manner. The innovations of this article are summarized as follows:

1. We have developed a credibility evaluation model for UWB ranging measurements to assess their quality. Credibility is defined as the probability that the positioning accuracy falls below 1m when the ranging result is directly utilized for positioning. This model uses the CIR sequence as input, and the ranging measurement error as correlation factors to establish a mapping relationship between ranging measurement and its credibility. By further extracting high-precision ranging results based on channel identification, this approach maximizes the benefits of UWB technology. It ensures the accuracy of positioning data used directly, enhances subsequent ranging error mitigation, and improves overall positioning performance.
2. We categorize NLOS ranging measurement errors into three detailed categories based on the fundamental causes of errors and variations in the CIR waveform. By credibility evaluation, we directly employ high-credibility and high-precision ranging results for localization, discarding low-credibility and uncorrectable ranging outcomes. For the remaining low-credibility data with valuable correction potential, this paper develops a ranging error mitigation model using a BERT-LSTM framework. This model inputs a two-dimensional vector comprising the CIR sequence and CIR features, thereby considering both temporal and energy information simultaneously. This approach addresses the limitations of traditional models, which typically capture only single-dimensional temporal or energy information.
3. We extend the error correction to LOS data unlike traditional algorithms that focus on correcting NLOS data only. The LOS ranging results are categorized into two groups based on the error causes and an error correction strategy of retaining, correcting as well as discarding is adopted based on the credibility evaluation. This expanded correction scope includes LOS data that may have been misclassified as NLOS or are impacted by multipath interference, thus enhancing the accuracy of these low-precision measurements and preventing their direct use in positioning, which could otherwise reduce accuracy. In addition, this strategy minimizes the dependence of ranging error mitigation and localization accuracy improvement on channel identification performance. We validated the effectiveness of our proposed credibility evaluation and ranging error mitigation models through both dynamic and static experiments across various scenarios, confirming their positive impact on localization accuracy.

2. Literature review

Existing algorithms for suppressing NLOS ranging measurement errors can be categorized into two types: multi-source fusion and error correction. Multi-source fusion algorithms do not correct NLOS ranging measurement errors but instead suppress their impact on positioning accuracy by incorporating additional information to calculate the positioning result. Venkatesh and Buehrer [8] uses LOS ranging measurements to define the objective function and NLOS ranging measurements to constrain the feasible domain, solving for coordinates through linear programming. When the density of UWB anchors is sufficient, Chen [9] employs residual weighted fusion of ranging measurements from different channels to suppress NLOS errors. Jiao et al. [10] further reduces computational demand by selecting the minimal combination of residuals, achieving a 58.91% reduction in data computation. These algorithms are ineffective in LOS-free environments, and their localization accuracy depends on the percentage of LOS ranging measurements. Additional information can also from other localization techniques. Articles [11, 12] combine UWB localization with fingerprint matching of wireless signals (Wi-Fi, BLE) and ranging [13] or angular [14] localization to mitigate NLOS errors. However, the effectiveness of these algorithms is limited by the inherent accuracy and coverage of wireless signal localization. Vandermeeren and Steendam [15] employs filtering techniques to fuse real-time IMU data with UWB localization results, enhancing accuracy in NLOS environments. Standalone UWB localization accuracy was 0.63 m but improved to 0.34 m and 0.41 m with Kalman Filter and Particle Filter fusion algorithms, respectively. This accuracy further improved to 0.28 m after incorporating map information [16]. However, IMU cumulative error in continuous NLOS environments can drastically reduce the positioning accuracy of the fusion algorithm, necessitating high-resolution road network information for additional map constraints. Lin and Zhan [17] used a nonlinear optimization method with loose coupling to improve the localization accuracy of the fusion algorithm to 20 cm by combining local pose estimation of visual inertial odometry based on UWB short-term position optimization with global constraints. The high accuracy of visual positioning and the additional map information it provides can significantly suppress UWB

localization drift under NLOS conditions. However, obstacles and pedestrian movement can significantly degrade visual localization performance. Multi-source fusion NLOS ranging measurement error suppression algorithms are less dependent on a priori information and can significantly improve localization continuity and performance under NLOS. However, integrating multiple techniques increases system complexity and reduces fault tolerance, and the limitations of additional techniques constrain the algorithm's applicability.

The correction of NLOS ranging measurement errors utilizes UWB information to enhance measurement accuracy. In the UWB NLOS ranging process, the CIR sequence includes the true first path (FP_T, representing actual ranging measurements), the report first path (FP_R, representing erroneous ranging measurements), and additional information such as the environmental layout and obstacles. Therefore, estimating the FP_T from the sequence CIR can correct the NLOS ranging measurements from the source. Heidari and Pahlavan [18] processed the CIR sequence with a finite bandwidth filter to enhance the differentiation of different path signals and re-estimate the ranging measurements. Dardari et al. [19] utilized the relative magnitude and distance (defined as rank) of different path CIRs instead of the original magnitude and re-estimated the ranging measurements based on a sequence of statistical ranks. These algorithms transform the original CIR and re-search for the FP_T, but traversing all CIR samples is time-consuming, and the threshold for re-estimating the FP_T lacks robustness. Deep learning can self-learn ranging measurement error-related information from CIR sequence without modifying the original data. Gao et al. [21] reduced the Mean ranging measurement error from 3.65 cm to 0.27 cm by combining CNN with CIR sequences, but the experimental environment had only weak NLOS interference with localization error within 30.00 cm. CNN focuses more on the local features and spatial information of the CIR sequences and is unable to establish the global features of long CIR sequences. In typical indoor scenarios such as offices and corridors, LSTM can improve the average positioning accuracy by 62% [22] compared to the original ranging measurements combined with least squares, with its prediction error differing from the actual error by an average of 0.028 m. Using the same CIR sequence as input [20], the mean and root mean square error (RMSE) of NLOS ranging measurement error after LSTM correction are 5.9% and 5.1% higher, respectively, than those of CNN. LSTM is more adapted to the information of CIR sequences, but its step-by-step processing method is slower in training and has gradient anomalies that affect information propagation. Nkrow et al. [23] divides NLOS measurement errors into hard NLOS and soft NLOS and constructs a CNN-LSTM error correction algorithm. In the two scenarios mentioned above, the error RMSE after CNN-LSTM correction is 9.5% and 4.7% better than that of CNN, respectively. Deep learning algorithms can intuitively extract ranging measurement errors from CIR sequences; however, redundant data, inefficient traversal of the input data, and the fact that CIR sequences contain fewer energy features constrain the performance of ranging measurement error correction. Machine learning can construct mapping relationships between artificial CIR features from CIR sequence data and ranging measurement errors. Yu et al. [24] showed that combining ranging measurements with a feature vector containing two CIR features as input to SVM can reduce the Mean and RMSE of UWB ranging measurement error by 59.8% and 49.3%, respectively. However, the performance of this feature vector in the environment of article [25] decreases by 3.1% and 13.5%, respectively. The optimal feature vector at this time contains five CIR features and keeps the Mean and RMSE of the ranging measurement error below 0.1m and 1.5m, respectively. The maximum difference in performance between differently composed feature vectors is 3.12% [25]. The machine learning algorithm needs to adjust the feature vector composition according to different environments to ensure error correction performance and focuses more on energy information because it cannot incorporate the CIR sequence. Ranging measurement error correction algorithms can correct the ranging measurement from the source to improve accuracy, but the existing algorithms cannot simultaneously account for the timing (CIR sequence) and energy information (CIR feature) related to the error. NLOS ranging measurement errors arise from various sources, including both high-precision measurements that meet positioning requirements and low-precision measurements lacking correction values. Applying a uniform correction model to these diverse errors fails to optimize ranging accuracy and may even degrade the accuracy of some high-precision measurements. To overcome the limitations of existing algorithms, this paper constructs an UWB ranging measurement credibility evaluation system designed to distinguish between high-precision, valuable correction measurements and worthless correction measurements. Additionally, it utilizes a BERT-LSTM model that incorporates both temporal and energy information to optimize ranging measurement errors caused by different factors.

3. Backgroud

3.1. UWB Ranging Principle

UWB technology uses narrow sine pulses ranging from nanoseconds to picoseconds for communication and data transmission. It measures the signal arrival time at different devices based on high time resolution to calculate the time of flight and corresponding ranging measurements (d). The core of measurement accuracy is the precise identification of signal arrival time [26]. Based on the built-in Leading Edge Detection (LDE) algorithm [27], UWB estimates environmental noise using the CIR generated in real-time during the ranging measurement process and determines the first CIR that exceeds the dynamic threshold (LDE_{thre}) as FP_R. CIR is the sum of multiple attenuated and delayed replicas of UWB pulses, recording the arrival time and energy attenuation of different paths signals. Figure 1 illustrates that the CIR sequence includes FP_T, which corresponds to the real ranging measurement ($\hat{d}$), and FP_R, which corresponds to

the ranging measurement(d) with an error(e). Therefore, the e, excluding any offset, is the absolute difference between $\hat{d}$ and d.

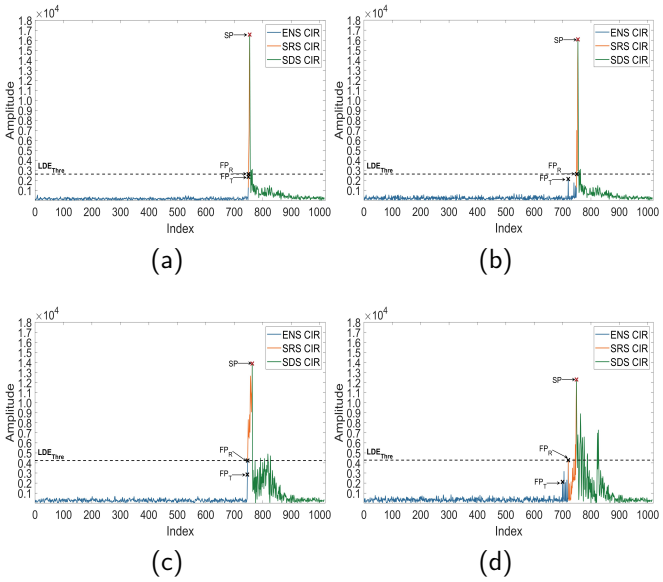

Figure 1: The typical UWB CIR sequence for different ranging, (a) LOS^H, (b) LOS^S, (c) $NLOS^S$, (d) $NLOS^H$.

Based on the FP_R and the strongest path signal (SP) in multipath signals, the CIR sequence can be divided into three stages: Environment Noise Stage (ENS) $[1 : FP_R]$, CIR Steep Rise Stage (SRS) $[FP_R + 1 : SP]$, and CIR Slow Descent Stage (SDS) $[SP + 1 : End]$. The ENS phase is characterized by stable and naturally fluctuating environmental noise. With the arrival of the UWB signal, the CIR rises and falls after the peak as the multipath signal (MP) propagation distance increases. LOS has weak multipath effects, while CIR rises sharply in the SRS stage and slowly decreases in the SDS stage. The difference between FP_T and FP_R in the LOS diagram is relatively small due to the negligible impact of hardware algorithm system delay on accuracy. NLOS obstacles will attenuate FP_T, and when its energy cannot meet the dynamic LDE_{thre}, it will cause FP_T and subsequent MP to be classified as ENS, further increasing LDE_{thre}. UWB will mistakenly identify a subsequent high-energy MP as FP_R, and the difference between FP_R and FP_T becomes the ranging measurement error (e). As shown in SRS, the severe multipath effect lead to a slow rise of CIR and a further increase in ranging error.

Due to variations in the attenuation of FP_T caused by different obstacle materials (e.g., conductivity, dielectric constant, magnetic permeability) and physical properties (e.g., density, thickness, porosity), this paper categorizes the theoretical low-precision NLOS ranging measurements into NLOS soft ($NLOS^S$), NLOS middle ($NLOS^M$), and NLOS hard ($NLOS^H$). When obstacles like glass or wooden boards cause minimal UWB signal attenuation, allowing FP_T to satisfy the dynamic Leading Edge Detector threshold (LDE_{thre}), the NLOS environment results in low ranging measurement errors, suitable for positioning. These measurements, similar to standard LOS CIR waveforms as depicted in Figure 1c, are classified as $NLOS^S$ and are characterized by high accuracy and the potential for direct use in positioning. When obstacles, such as human bodies or thin walls, increase the attenuation of UWB signals causing FP_T to fall short of the dynamic LDE_{thre} yet remain above environmental noise, the ranging measurement error is higher and unsuitable for positioning. As shown in Figure.1d, there are some abnormally high-energy CIR samples during the ENS phase. This type of measurement is classified as $NLOS^M$, characterized by lower-quality ranges. Although its accuracy is inferior to $NLOS^S$, it contains adequate error correction data within its CIR waveform. When obstacles, such as thick walls or metal, further increase the attenuation of UWB signals causing FP_T to fail to meet the dynamic LDE_{thre} and become indistinguishable from environmental noise, the effective communication signals between UWB devices mainly result from reflection and scattering. At this point, the ENS of the CIR sequence is similar to the standard LOS ENS, and the remaining stages are diverse due to the interference of multipath effects. At this point, the measurement categorized as $NLOS^H$ represents gross errors with the highest unknown and contains minimal accurate ranging data ability within its CIR sequence to be useful for positioning. In this case, $NLOS^H$ measurement data will mostly be discarded.

To summarize, the causes and magnitude of NLOS ranging measurement errors vary due to factors such as obstacles and environmental layout. Traditional definitions of LOS and NLOS focus only on the presence of obstacles in the straight path between devices and do not account for environmentally induced multipath effects. When the multipath effect is increased by the presence of metal around the device or interference from walls or other high-power devices, it enhances environmental noise and introduces ranging measurement error when FP_T cannot satisfy LDE_{thre}. Similar to $NLOS^M$, its FP_T is still significantly different from other environmental noise in ENS and can be effectively corrected. Based on this, this article divides LOS ranging measurements into LOS hard (LOS^H in Figure.1a) similar to $NLOS^S$, LOS soft (LOS^S in Figure.1b) similar to $NLOS^M$. The ranging error of LOS^S is from the mulitpath errors. It is necessary to optimize for different types of NLOS and LOS ranging measurement errors separately to achieve maximum accuracy improvement.

3.2. Bidirectional Encoder Representations from Transformer

The Transformer [28], at the core of the Chat Generative Pre-trained Transformer (ChatGPT), is a neural network architecture based on the self-attention mechanism [29] and has been demonstrated in natural language processing, computer vision, and multi-modal tasks. On this basis, Bidirectional Encoder Representations from Transformers (BERT) [30] efficiently extracts local features and long-range dependencies (globally) of the same and different sequence

elements by executing multiple self-attention in parallel and independently of each other with a multi-head self-attention mechanism. Its deep bidirectional learning capability mines the feature information of input data more deeply than the Transformer. As shown in Figure2, BERT consists of two parts: the Embedding (WordPiece + Segment + Position) and the Encoder stack. The Embedding adds a special symbol [CLS] at the beginning of the multidimensional input ($X \in \mathbb{R}^{L\times 1}$) and separates different dimensional inputs with the special symbol [SEP], converting X into $Y \in \mathbb{R}^{L\times d_{emd}}$, which is the input for the Encoder stack. L is the total length of the multidimensional input after adding special symbols, d_{emd} is the feature dimension parameters of BERT. The three components of Embedding consist of two steps: numerical assignment and learning extension. The value of WordPiece is a unique integer assigned by the corpus for each input. The value of Segment indicates the sequence to which the input belongs, with identical values for inputs within the same sequence. The value of Position represents the input's location, utilizing a sine function instead of recursion and convolution to capture the sequence's temporal information. After each Embedding assigns a unique numerical value to the input, it is expanded into a high-dimensional vector during the learning process, thereby enhancing its target information. For the credibility evaluation, when using the CIR sequence and ranging results as inputs, BERT effectively captures both the temporal and energy correlations among CIR samples within the sequence and between each CIR sample and the ranging results. Similarly, for ranging error mitigation employing the CIR sequence and CIR features as inputs, BERT comprehensively acquires the ranging error timing and energy information of the CIR sequence, as well as the specific ranging error information contained in each CIR feature. Moreover, its deep bidirectional learning capability facilitates the extraction of detailed CIR features and the associated ranging information. The final Y is the sum of the three vectors, resulting in a dimension of $L \times d_{emd}$. The Encoder stack is composed of C superimposed encoders, which perform feature extraction on Y and form an output feature vector $Z \in \mathbb{R}^{L\times d_{emd}}$, and adjust the weight of each encoder according to the target task.

Each Encoder layer comprises a multi-head self-attention mechanism (MAT) and a position-wise fully connected feed-forward network (FFN), interconnected through layer normalization with residual connections (NR). The MAT consists of D Scaled Dot-Product Attention units (AT), with inputs being Queries ($Q \in \mathbb{R}^{L\times d_k}$), Keys ($K \in \mathbb{R}^{L\times d_k}$), and Values ($V \in \mathbb{R}^{L\times d_v}$), obtained by multiplying the output of the previous layer with the corresponding weight matrices ($W^Q \in \mathbb{R}^{d_{emd}\times d_k}$, $W^K \in \mathbb{R}^{d_{emd}\times d_k}$, and $W^V \in \mathbb{R}^{d_{emd}\times d_v}$, where $d_k = d_v = d_{emd}/C$). The Scaled Dot-Product Attention (AT) is defined as follows:

$$AT(Q,K,V) = softmax(\frac{Q\times K^T}{\sqrt{d_k}})V \quad (1)$$

The AT first combines Q and K to form an attention graph matrix of size $L \times L$. The weight information in the upper right corner of the attention map matrix is eliminated to ensure that each piece of data knows only its own and the preceding data's attention weights. Gradient anomalies are prevented by scaling with $\sqrt{d_k}$ and performing weight normalization operations, then combining with V to form the final attention matrix. The MAT result, consisting of the superposition of AT units, is as follows:

$$MAT(Q,K,V) = Concat(AT_1,\dots,AT_D)W^O, \quad (2)$$

where $W^O \in \mathbb{R}^{(D\times d_v)\times d_{emd}}$ is the parameter matrix of the MAT. During the learning process, by adjusting the weight matrix, the model can focus more on information with higher weights that affect the target task(ranging credibility evaluation and error mitigation). After NR, the output is passed to the next sub-layer of the Encoder, which is a fully connected feed-forward neural network (FNN) consisting of two linear transformations connected by ReLU activation, as described by the following equation:

$$FFN(NR(MAT)) = max(0, NR(MAT) * W_1 + b_1)W_2 + b_2 \quad (3)$$

where W_1 and W_2 are size of $d_{emd} \times d_{ff}$ and $d_{ff} \times d_{emd}$, respectively; b_1 and b_2 is the parameter. The FNN initially maps features derived from the multi-head attention matrix linear transformation into a high-dimensional space, then reduces them to a low-dimensional space, effectively learning more relevant features for the target task through nonlinear activation functions. After NR, the output ($NR(FNN)$) is passed to the next Encoder. After the input vector Y passes through C Encoders, we obtain the result vector

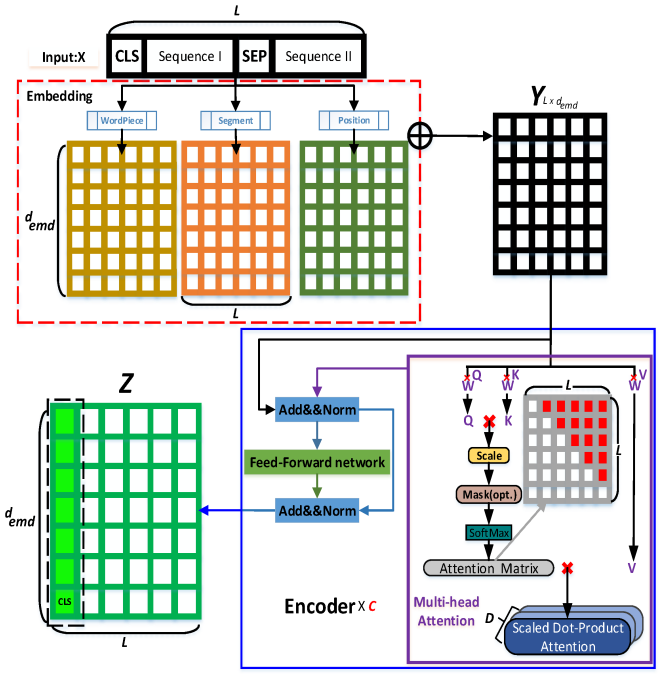

Figure 2: The structure of BERT includes Embedding and Encoder stack, as well as the process of converting input data into feature vectors.

$Z \in \mathbb{R}^{L \times d_{emd}}$, which contains a special label Z_{CLS}. The Z_{CLS} token not only marks the beginning of the entire input sequence but also encapsulates key feature information, such as ranging credibility and error mitigation, for the entire sequence Z. To fully capture the ranging error and credibility evaluation information embedded in the time-correlated CIR sequence data, the proposed algorithm employs an LSTM layer after BERT to enhance the model's ability to extract temporal information from the sequence and identify additional nonlinear features. Finally, the regression layer is used to achieve credibility evaluation and correction of the ranging error.

4. Proposed Methodology

As shown in the Figure.3, this paper divides UWB ranging measurements into identified LOS (I-LOS) and identified NLOS (I-NLOS) based on channel identification results. The channel identification algorithm proposed in this paper utilizes BERT [31] in conjunction with the CIR sequence to differentiate between I-LOS and I-NLOS conditions. Obstacles attenuate UWB signals, leading to significant differences in the amplitude and time delay of theoretical LOS (Figures 1a, 1b) and theoretical NLOS (Figures 1c, 1d) waveforms. BERT leverages deep bidirectional learning of LOS and NLOS features in combination with CIR sequences to accurately identify I-LOS and I-NLOS. By analyzing CIR waveforms corresponding to different error sources, we conduct a fine-grained classification of LOS and NLOS ranging measurements using CIR features. Through simulation experiments and empirical data, we develop a credibility evaluation system for ranging measurements using a BERT-LSTM model. Using the proposed credibility evaluation model, we implement a strategy for NLOS data to recall high-credibility, high-precision ranging measurements, discarding low-credibility, non-useful measurements, and correcting valuable ones. This approach maximizes the retention of valuable and directly applicable ranging measurements, fully leveraging the advantages of UWB ranging measurements. For various error sources, BERT-LSTM is employed to optimize ranging measurements by incorporating both the CIR sequence timing information and CIR features energy information. Additionally, this paper extends error correction to LOS measurements, reducing the reliance of subsequent positioning accuracy on channel identification performance.

4.1. UWB ranging measurement credibility evaluation

The credibility of UWB ranging is defined as the probability of producing positioning results below 1 meter when the ranging data are directly utilized for positioning, with scores ranging from 0 to 1. A higher score signifies greater accuracy. The inherent advantages of UWB allow even partially attenuated NLOS signals to satisfy positioning requirements. Completely discarding useful NLOS signals would negate the benefits of UWB, while attempting corrections could compromise the accuracy of such data. Due to the presence of misclassification, data labeled as LOS after NLOS classification stage might include misclassified NLOS data and inherently low-precision LOS ranging results. Using all LOS-labeled data directly for positioning can reduce positioning performance. The accuracy of UWB ranging is intrinsically linked to the ultimate positioning accuracy. The credibility evaluation guided by positioning accuracy, as proposed in this paper, effectively extracts high-precision ranging results, ensuring positioning accuracy while reducing reliance on channel identification performance.

Due to the absence of a credibility calculation method in existing research and the challenges of collecting ranging measurements with varying error levels in real-world environments, this paper employs simulation experiments to define the credibility associated with different ranging measurement errors. The measurement categories LOS^H, LOS^S, $NLOS^S$, $NLOS^M$, and $NLOS^H$, as defined in Section 3.1, represent ranging results with varying accuracy levels due to differing degrees of obstacle interference and multipath effects. As such, there is a need to ascertain the credibility in the usage of these ranging signals. Our proposed credibility evaluation algorithm selects an error range of 0.001 m to 5.00 m to encompass these different types of ranging results [32, 33]. Furthermore, our proposed credibility evaluation algorithm has been ascertained in our three experimental scenarios. Ranging results within 0.001 m to 0.10 m are classified as high-precision and can be directly used for positioning without requiring correction. These results primarily correspond to the LOS^H and most of the $NLOS^S$. As errors increase within the range of 0.10 m to 0.80 m, the credibility of the ranging results decreases, necessitating correction before they can be utilized for positioning. This range is predominantly associated with most of the theoretical $NLOS^M$ and LOS^S. When errors exceed 0.80 m and extend up to 5.00 m, the accuracy and correctability of the ranging results significantly deteriorate, corresponding to the theoretical $NLOS^H$ described in this study. In these simulations, three UWB anchors and one tag are randomly placed within the simulation area. The true ranging measurement from the tag to each anchor is calculated based on their coordinates. As illustrated in Figure 4, ranging measurement errors are incremented from 0.001 m to 5.00 m at intervals of 0.001 m for one of the three ranging measurements, while the other two remain accurate. This process is repeated for the other two ranging measurements, generating a total of 3×5000 datasets, each containing two accurate measurements and one with an introduced error. The deviation between the positioning result with introduced errors and the actual positioning result is then calculated. This experiment is repeated 500 times across the simulation area, yielding a total of 7.5 million datasets. The credibility of a ranging measurement error is defined as the percentage of cases where positioning errors are less than 1 meter under this error condition. Figure 4 illustrates the distribution of ranging measurement errors and their corresponding credibility in the simulated experiments. The

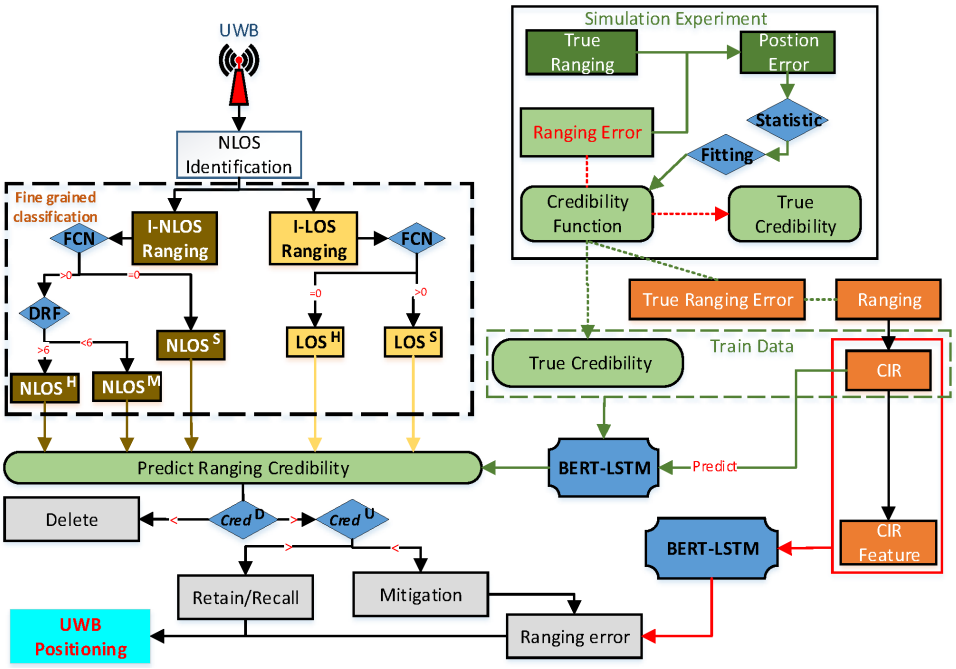

Figure 3: The structure of the proposed algorithm includes Ranging Credibility, Fine grained classification, and Ranging mitigation, as well as the process of optimizing UWB ranging and positioning.

resulting curve represents the credibility function, which provides the true credibility corresponding to each ranging measurement error.

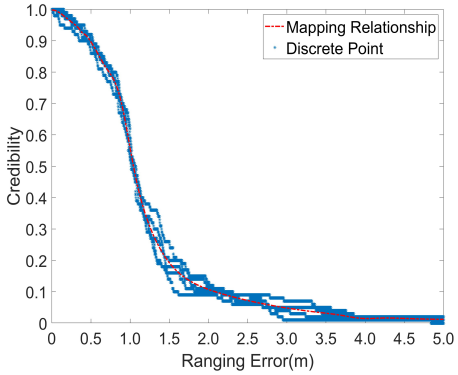

Figure 4: The mapping relationship between UWB ranging measurement error and credibility in simulation experiments.

In a multi-scenario testing environment, this paper determines the true position of the tag through high-precision visual positioning and calculates the error contained in each UWB ranging measurement. As shown in the Figure.4, the credibility equation from the simulation experiment is used to obtain the true credibility corresponding to the ranging result. Based on the previous analysis, the sequence CIR contains the ranging measurement error information that serves as a link for credibility evaluation. Consequently, this paper constructs a credibility evaluation model based on BERT-LSTM, using the CIR sequence and ranging measurements as inputs. By extracting local and global features through BERT and enhancing the weight of ranging measurement error timing information with LSTM, the accuracy of credibility estimation is improved. Additionally, due to the different proportions of low-error data in LOS and NLOS ranging results, LOS contains more high-reliability measurements, while NLOS contains more low-reliability measurements. To accurately evaluate the credibility of ranging measurements, this paper constructs separate credibility evaluation models for LOS and NLOS structures. Credibility helps algorithms retain high-precision ranging measurements to maximize the advantages of UWB ranging and positioning. For ranging measurements that cannot be directly used for positioning, this paper improves ranging measurement accuracy through fine-grained classification and the development of corresponding optimization strategies.

4.2. Ranging Classification and Mitigation

For fine-grained ranging Classification, we uses the CIR features such as the False Crests Number (FCN) and the difference between RPL and $FPPL$, denoted as $DRF = RPL - FPPL$ [26]. FCN represents the count of abnormally high-energy CIR samples that surpass the threshold ($LDE_{thre} * 0.6$) during the Environmental Noise Stage. An FCN of zero indicates no abnormal energy in the environmental noise, suggesting a waveform close to a standard LOS condition with minimal ranging error. Conversely, an FCN greater than zero signifies the presence of high-energy anomalies in the environmental noise, including the true first path signal, multipath signal, and environmental noise anomalies, which lead to significant ranging errors. As illustrated in Figure.3, we employ FCN to finely classify I-LOS into high-accuracy LOS^H and low-accuracy LOS^S.

For I-NLOS, we initially classify those with FCN equal to zero as $NLOS^S$, indicating no high-energy abnormal CIR in its environmental noise. For other datasets, where there is abnormally high energy in the environmental noise, the error correlates more with the signal attenuation level. DRF, which measures the degree of signal attenuation, suggests that a lower value indicates lesser attenuation. When DRF is below 6[26], it is classified as $NLOS^M$, indicating less energy attenuation and higher accuracy in the data with $FCN > 0$. Conversely, a higher DRF classifies as $NLOS^H$, indicating greater energy attenuation and reduced accuracy.

The classification principle focuses on the presence of high-energy abnormal CIR samples during the ENS phase and the energy attenuation of the main signal. However, the degree of multipath interference, along with the quantity and amplitude of high-energy abnormal CIR samples, can significantly affect ranging measurement accuracy. Therefore, the overall accuracy of the three types of ranging measurement errors after fine-grained classification by CIR features ranges from high to low, but each type of ranging error consists of high-precision uncorrected data, low-precision valued and valueless corrected data, only in different proportions. As shown in Figure 3, this paper establishes reliability thresholds: credibility up ($Cred^U$) and credibility down ($Cred^D$) for each type of ranging result. Data with credibility exceeding $Cred^U$ will be retained (recalled), those below $Cred^D$ will be deleted, and the remaining data will be considered for mitigation.

For valuable correction data, the focus is on the first path evaluation, which separates FP_T from CIR sequences containing environmental noise and MP. Given the temporal information preference of CIR sequences, this paper introduces features such as First Path Error (FPE), the mean amplitude of CIR sequences (r_{mean}), mean excess delay (τ_{med}), and root mean square delay (τ_{rms}) to enhance energy information and calculate error correction (Δd) for the LDE algorithm. FPE represents the time difference between the re-evaluated first path signal, optimized for environmental noise estimation, and the LDE algorithm's first path signal. For $NLOS^S$ and $NLOS^H$, which lack high-energy abnormal CIR during the ENS phase, r_{mean} is used to measure environmental noise intensity, while τ_{med} assesses the strength of multipath signals in the CIR sequence. As shown in Table.1, mitigation model can learn FP_T information embedded in CIR sequences and features, correlating it with known ranging measurements through the parameter FPE, ultimately yielding Δd. In cases of $NLOS^M$, where abnormal energy CIR is present in the ENS phase, r_{mean} becomes unsuitable for estimating environmental noise due to the significant differences between FP_T, MP, and environmental noise. Therefore, only τ_{med} is necessary to assist model in distinguishing MP.

Existing algorithms directly use I-LOS for positioning, limiting the improvement in positioning accuracy achievable through ranging measurement correction algorithms to channel identification accuracy. This limitation arises because the channel identification algorithm cannot completely separate true LOS and NLOS ranging measurements, leading to partial misjudgment of true NLOS measurements as I-LOS. Additionally, some true LOS ranging measurements are affected by multipath effects and contain errors, necessitating the classification and optimization of LOS to enhance positioning accuracy. As shown in Figure.3, this article uses FCN to divide LOS into LOS^H and LOS^S, and further refines them into categories of preservation, valuable correction, and worthless correction based on credibility evaluation. Similar to $NLOS^S$, this article uses r_{mean} and τ_{rms} to evaluate environmental noise and multipath signal levels of LOS^H, combining them with FPE to obtain Δd. In contrast, analogous to $NLOS^M$, r_{mean} is discarded for calculating environmental noise and τ_{rms} is used to evaluate multipath signals for LOS^S. The ranging measurement error mitigation model is the fusion of BERT and LSTM. BERT can process multidimensional inputs composed of CIR features and sequences, simultaneously accounting for the temporal and energy information of ranging measurement errors. Since ranging measurement errors result from the delay in detecting the first path signal, BERT is combined with LSTM to enhance the capture of temporal information.

Table 1
CIR features and CIR sequences for UWB ranging measurement error correction

Type	CIR features	CIR sequence
$NLOS^S$	$FPE, r_{mean}, \tau_{med}$	N1:N2
$NLOS^M$	FPE, τ_{med}	N1:N2
$NLOS^H$	$FPE, r_{mean}, \tau_{med}$	N1:N2
LOS^H	$FPE, r_{mean}, \tau_{rms}$	N1:N2
LOS^S	FPE, τ_{rms}	N1:N2

It is important to note that the thresholds used for classification have been empirically derived from various sources, including relevant literature and UWB device manufacturers [26, 34], as well as our own experimental studies. These thresholds are applicable to any UWB devices that utilize CIR-related parameters for ranging and localization. Additionally, the BERT model we propose for ranging error mitigation will integrate classified paths under one of these five LOS/NLOS categories with CIR features and the CIR sequence. This integration minimizes misidentification during LOS/NLOS ranging error mitigation, even when the thresholds are not empirically optimal.

5. Experiment

To verify the performance of the proposed credibility evaluation model and ranging measurement error correction strategy, as well as the improvement in dynamic positioning accuracy, experiments were conducted in three scenarios: the State Key Laboratory of Satellite Navigation System and Equipment Technology of the 54th Research Institute of China Electronics Technology Corporation (LAB);

the School of Environment and Spatial Information, China University of Mining and Technology (CUMT); and the Industrial Internet of Things laboratory at IDLab, Ghent University (UGent). The UWB module is based on IEEE 802.15.4-2011, with a communication rate of 110 kb/s, an effective communication distance of 50 m, a working center frequency of 3.5 GHz, and a transmission power of -41.3 dBm/MHz.

As depicted in Figure 5a, during LOS data collection, both the UWB anchor and tag are located in the open area on the first floor of the LAB. For the NLOS data collection, the UWB anchor is positioned on the second floor while the tag remains on the first floor, with UWB signals obstructed by glass and walls. This setup simulates the localization performance of the proposed algorithm in urban canyons and shopping centers. Figure 5b shows that during LOS data collection in the CUMT corridor, space constraints lead to enhanced multipath effects compared to the LAB. For NLOS data collection, the anchor is in the corridor, and the tag is in a room, with obstacles including wooden doors, tables, and chairs. This scenario simulates the algorithm's localization performance in teaching buildings. UWB tags remain at each predefined location for 10 minutes, collecting 50 LOS CIR sequences and 50 NLOS CIR sequences per minute. As illustrated in Figure 5c, LOS data collection occurs near desks and chairs surrounded by office supplies. NLOS data collection includes two scenarios: the first (NLOS-1) involves obstacles such as walls and electronic devices (displays, computer towers) to simulate signal interference, termed UGent-1. The second (NLOS-2) involves arranging personnel movement in the vicinity to enhance interference, termed UGent-2. UGent represents an office environment where the two NLOS scenarios correspond to fixed obstacles and dynamic human interference, simulating libraries or crowded spaces. The true ranging results obtained through high-precision vision positioning. For the three scenarios across four experimental sets, the data volumes are 14734, 15298, 12844, and 13896, respectively. For each experiments, the collected data is divided into training and testing in a ratio of 70:30.

5.1. Credibility Evaluation

In multiple scenarios, the Mean predicted credibility error ($Cre^e = |Cre^p - Cre^t|$) between predicted credibility (Cre^p) and true credibility (Cre^t) is 0.045, with a standard deviation (STD) of 0.065 and a root mean square error (RMSE) of 0.120. As shown in Table.2, the Cre^e in the NLOS fluctuates between 0.052 and 0.082, with an Mean of 0.066, and the maximum difference across scenarios is 0.030. The Cre^e under LOS ranges from 0.019 to 0.032, with an Mean of 0.024, and the maximum difference across scenarios is only 0.013. Compared to the NLOS environment with multiple obstacles, the LOS environment can be uniformly regarded as channel scenes with air as the propagation medium. Therefore, compared to the widespread distribution of ranging errors in NLOS environments, LOS

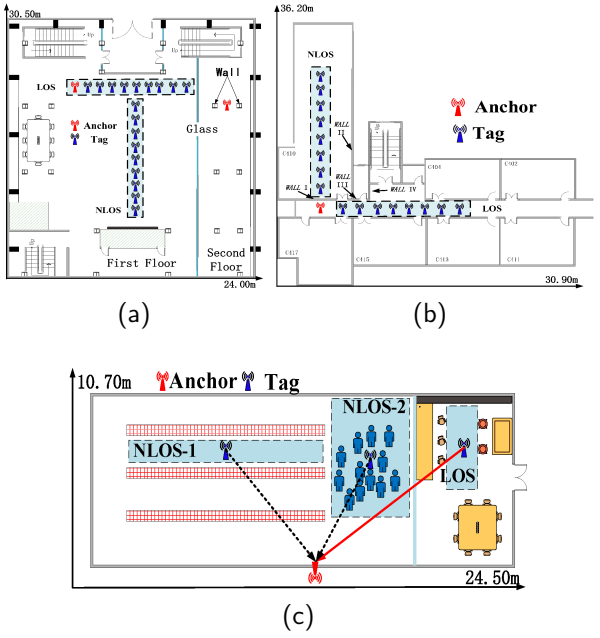

Figure 5: The Experimental testing environment and anchor layout, (a) LAB, (b) CUMT,(c) UGent.

environments have lower ranging errors and higher credibility, resulting in more accurate model predictions. Even from the UGent test field with a stable channel environment to the CUMT corridor with strong multipath and the LAB test field with severe wireless signal pollution, the Cre^e only increased by 0.001(0.011) and 0.016(0.027) in LOS(NLOS), respectively. The performance and robustness of the proposed credibility evaluation model have been validated in different scenarios and meet expectations.

Table 2
The Cre^e under different scenarios.

	Channel	Mean	Std	Rmse
LAB	LOS	0.032	0.074	0.107
	NLOS	0.082	0.095	0.176
CUMT	LOS	0.020	0.019	0.095
	NLOS	0.071	0.061	0.108
UGent-1	LOS	0.019	0.056	0.099
	NLOS	0.058	0.119	0.157
UGent-2	LOS	0.023	0.040	0.090
	NLOS	0.052	0.058	0.131

Table.3 shows the preset ranging measurement error range corresponding to Cre^t in four credibility levels ([1.00, 0.99], (0.99, 0.97], (0.97, 0.95], (0.95, 0.00]), as well as the mean actual ranging measurement error corresponding to Cre^p. In four credibility levels, the mean ranging measurement error corresponding to Cre^p are 0.071m, 0.182m, 0.288m, and 1.426m, all of which meet the preset ranging measurement error range. Among them, only the mean ranging measurement errors of LAB exceeded the preset

ranges [1.00, 0.99] and (0.99, 0.97], respectively, by 0.012m and 0.018m. Figure.6a, 6c, 6e and 6g show the distribution of ranging measurement errors within the four credibility levels, mainly concentrated in 0.032-0.099m, 0.103-0.185m, 0.218-0.318m, and 0.758-1.946m, all meeting the preset target. Within the four credibility levels, at most one scenario had a ranging measurement error distribution exceeding the preset range, with exceedances of about 0.05m. The highest being CUMT exceeding 0.068m within the (0.97, 0.99) credibility range, and the lowest being CUMT exceeding 0.03m within the (0.95, 0.97) credibility range. Overall, the ranging measurement error corresponding to the Cre^p in LOS scenarios has achieved the expected goal, ensuring the maximum extraction of high-precision ranging measurements. Although the prediction of high-reliability ranging measurement error is lower than the preset target, it is more conducive to ensuring the accuracy of direct positioning data in practical applications.

Table 3
Ranging error corresponding to $Cred^p$

LOS	[1.00, 0.99]	(0.99, 0.97]	(0.97, 0.95]	(0.95, 0.00]
Error	0-0.09	0.09-0.21	0.21-0.31	≥ 0.31
LAB	0.102	0.228	0.303	1.554
CUMT	0.068	0.186	0.299	1.478
UGent-1	0.062	0.151	0.253	1.352
UGent-2	0.053	0.162	0.295	1.321
NLOS	[1.00, 0.95]	(0.95, 0.90]	(0.90, 0.80]	(0.80, 0.00]
Error	0-0.31	0.31-0.47	0.47-0.71	≥ 0.71
LAB	0.303	0.442	0.708	3.919
CUMT	0.256	0.449	0.632	3.226
UGent-1	0.306	0.418	0.755	2.837
UGent-2	0.292	0.431	0.636	2.981

In four credibility levels([1.00, 0.95], (0.95, 0.90], (0.90, 0.80), and (0.80, 0.00]), the mean ranging measurement error corresponding to Cre^p in multi-scenario NLOS channel are 0.289m, 0.435m, 0.683m, and 3.241m, respectively, all of which meet the preset ranging measurement error range. Among them, only UGent-1 had an average ranging measurement error exceeding the preset range at (0.90, 0.80) by 0.045m. As shown in Figure.6b, 6d, 6f and 6h The ranging measurement errors within the four credibility levels were mainly concentrated at 0.023-0.123m, 0.302-0.551m, 0.475-0.899m, and 1.843-4.77m, respectively. Except for the (0.90, 0.80) credibility level , all met the preset target. Within the (0.90, 0.80) credibility level, some of UGent's ranging errors were higher than 0.71m and exceeded the expected target. However, the probability of meter-level positioning results generated by ranging measurement errors at this time is low. Considering the NLOS channel environment, such data will not be directly used for positioning but will be used for ranging measurement error compensation. Therefore, it does not affect the credibility and subsequent application value. Overall, the average Cre^p in NLOS scenarios meets expectations, but as Cre^p decreases, model performance declines. However, low credibility data will not be directly used for localization, so it will not significantly impact localization accuracy. The credibility evaluation model proposed can assign accurate credibility to ranging results in both LOS and NLOS environments, ensuring the accuracy of direct use for positioning ranging results, and providing strong references for subsequent ranging measurement error correction and positioning, reducing dependence on channel identification accuracy.

5.2. Ranging measurement mitigation

Table 4 shows the mean ranging measurement error of retained and deleted (non-valuable correction) data based on credibility, as well as the mean raning measurement error of valuable correction data before (d^b) and after (d^a) correction. The Cre^U for LOS^H and LOS^S are 0.85 and 0.90, respectively. By optimizing the credibility range of retained data for different types of LOS measurements, the accuracy of ranging results used directly for positioning can be improved. The ranging measurement errors of high-credibility retained data in these two types of LOS measurements are concentrated within 0.05–0.06 m and 0.20–0.33 m, with mean errors of 0.064 m and 0.256 m, respectively. The Cre^D for LOS^H and LOS^S are 0.60 and 0.50, respectively. The mean errors of low-credibility deleted data in these two types of LOS measurements are 2.407 m and 2.016 m, respectively. Such measurements are either misclassified NLOS data or LOS data significantly affected by multipath interference. Due to their large errors and limited valuable information regarding FP_T in the corresponding CIR sequence, these data cannot be used for positioning and hold no correction value. The ranging measurement errors of the remaining data are concentrated at 0.53-0.58m and 0.59-0.69m, with average errors of 0.582m and 0.0.669m, respectively. This type of ranging measurement cannot be directly used for positioning, but due to its CIR waveform being more inclined towards standard LOS, indicating that UWB signals have a clear distinction from environmental noise, it has sufficient FP_T-related information to correct ranging measurement errors. Therefore, this paper uses BERT-LSTM combined with CIR sequences and CIR features to correct such data. The corrected ranging measurement errors are concentrated in 0.12-0.25m and 0.19-0.27m, with average errors of 0.194m and 0.258m, respectively, with reductions of 66.68% and 61.86%.

After implementing fine-grained classification, credibility evaluation, and targeted BERT-LSTM error correction, the overall ranging measurement error in I-LOS across multiple scenarios was reduced from 0.273 m to 0.175 m, representing an average reduction of 35.69%. The maximum absolute error reduction was 0.121 m in the UGent-1 scenario, while the highest reduction ratio was 40.09% in the CUMT scenario. As shown in Figures 7a, 7c, and 7e, the average proportion of m-level ranging measurement errors (errors less than 1 m) across multiple scenarios increased by 4.40%,

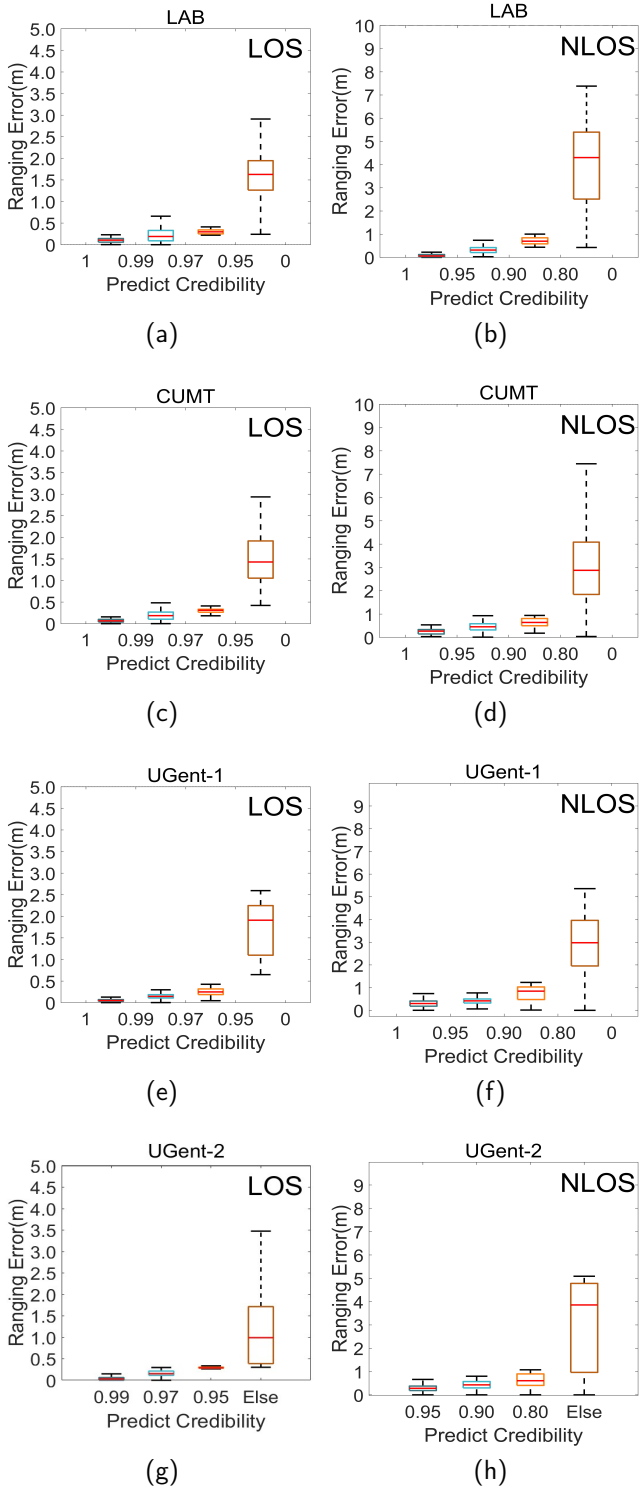

Figure 6: The ranging measurement error distribution corresponding to Cre^{p}, (a) LOS LAB, (b) NLOS LAB, (c) LOS CUMT, (d) NLOS CUMT, (e) LOS UGent-1,(f) NLOS UGent-1, (e) LOS UGent-2,(f) NLOS UGent-2.

reaching 99.1%, with a maximum increase of 7% observed in the LAB scenario. The average proportion of cm-level ranging errors increased by 12.46%, reaching 58.35%, with the maximum increase being 27.3% in the CUMT scenario. Notably, the proportion of cm-level ranging measurement errors (errors less than 0.1 m) after correction exceeded 50%, significantly enhancing the accuracy of positioning data. The proposed credibility evaluation method substantially improves the accuracy and reliability of positioning data. Furthermore, unlike traditional error correction strategies that are limited to NLOS data, the additional correction of LOS ranging results further enhances positioning accuracy and reduces the dependence of NLOS error correction performance and positioning accuracy on channel identification.

Table 4
LOS ranging measurement error correction performance

	Type	Keep	d^b	d^a	Delete
LAB	LOS^H	0.062	0.559	0.137	2.278
	LOS^S	0.304	0.596	0.265	1.896
CUMT	LOS^H	0.057	0.537	0.183	2.461
	LOS^S	0.329	0.603	0.254	1.983
UGent-1	LOS^H	0.050	0.576	0.251	2.395
	LOS^S	0.208	0.691	0.199	2.036
UGent-2	LOS^H	0.064	0.657	0.205	2.495
	LOS^S	0.182	0.669	0.258	2.147

Table.5 shows the mean ranging measurement error of recalled and deleted (non-valuable correction) data based on credibility, as well as the mean ranging measurement error of valuable correction data before and after correction. The Cre^U for $NLOS^S$, $NLOS^M$, and $NLOS^H$ are 0.80, 0.85 and 0.90, respectively. The ranging measurement errors of high-credibility retained data for these three NLOS categories are concentrated within 0.17–0.22 m, 0.18–0.28 m, and 0.25–0.34 m, with mean errors of 0.195 m, 0.224 m, and 0.302 m, respectively. The Cre^D for $NLOS^S$, $NLOS^M$, and $NLOS^H$ are 0.30, 0.40 and 0.50, respectively. The mean ranging measurement errors of low-credibility, uninformative data in these three NLOS categories are 3.169 m, 2.806 m, and 3.578 m, respectively. These data are significantly degraded by obstacles, resulting in large errors and limited information about FP_T in the CIR sequence. Deleting such data reduces computational power consumption and enhances the correction performance of valuable data. The ranging measurement errors of the remaining data are concentrated in 1.20-1.70m, 1.00-11.1m, and 1.2-1.5m, with Mean of 1.443m, 1.087m, and 1.406m, respectively. This type of ranging measurement cannot be directly used for positioning, but due to the presence of CIR, including FP_T or MP, which is significantly higher than environmental noise in its ENS stage, it contains sufficient ranging measurement error correction information. Therefore, this article uses BERT-LSTM combined with CIR sequences and CIR

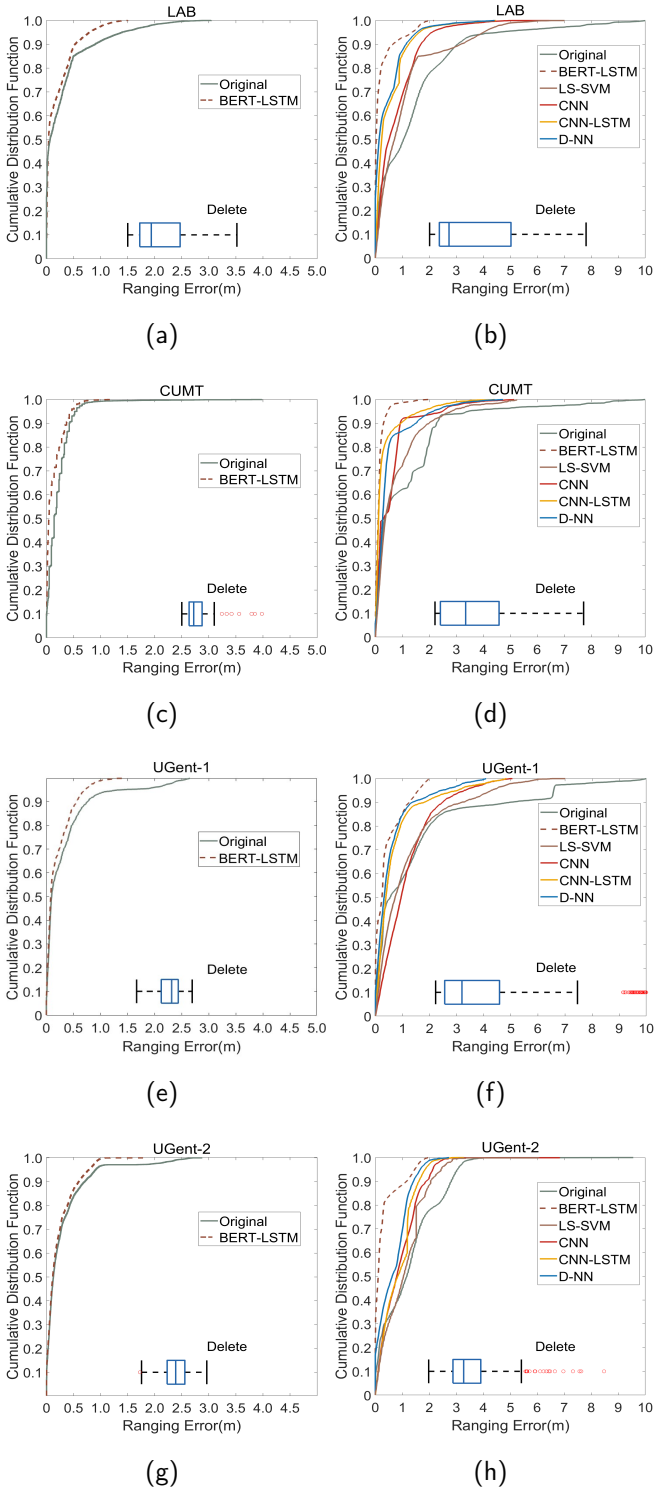

Figure 7: The distribution of ranging measurement errors before and after correction, (a) LOS LAB, (b) NLOS LAB, (c) LOS CUMT, (d) NLOS CUMT, (e) LOS UGent-1,(f) NLOS UGent-1, (g) LOS UGent-2,(h) NLOS UGent-2.

features to perform error correction on such data. The corrected ranging measurement errors are concentrated in 0.27-0.38m, 0.26-0.30m, and 0.25-0.34m, with average errors of 0.314m, 0.271m, and 0.269m, respectively, resulting in reductions of 78.21%, 75.12%, and 80.83%. The corrected ranging measurement error accuracy is similar to the recall data accuracy and can be used for subsequent positioning. By pre-retaining high-precision ranging measurements and deleting low-precision ones, the model can focus more on valuable error correction during training and maximize accuracy.

Table 5
NLOS ranging error correction performance

	Type	Keep	d^b	d^a	Delete
LAB	$NLOS^S$	0.178	1.212	0.275	3.296
	$NLOS^M$	0.185	1.119	0.261	2.244
	$NLOS^H$	0.252	1.290	0.265	3.681
CUMT	$NLOS^S$	0.217	1.202	0.373	2.096
	$NLOS^M$	0.284	1.097	0.276	3.937
	$NLOS^H$	0.338	1.314	0.256	3.562
UGent-1	$NLOS^S$	0.183	1.699	0.299	3.997
	$NLOS^M$	0.215	1.072	0.306	2.222
	$NLOS^H$	0.312	1.522	0.337	3.574
UGent-2	$NLOS^S$	0.203	1.657	0.310	3.291
	$NLOS^M$	0.212	1.060	0.239	2.819
	$NLOS^H$	0.304	1.498	0.220	3.495

As shown in Table.6, the overall ranging measurement error in I-NLOS across multiple scenarios was reduced from 1.296 m to 0.256 m, achieving an average reduction of 79.98%. The maximum reduction in absolute error was 1.20 m in the LAB scenario, while the highest reduction ratio was 85.71% in the LAB. As shown in Figure.7b, 7d, 7f and 7h, the Mean proportion of m-level ranging measurement errors in multiple scenarios increased by 38.01% to 91.87%, with the maximum increase being 43.95% for LAB. Compared to the original measurements, the maximum value of the 90% ranging measurement error decreased by 2.37m to 0.85m, with the maximum decrease being 3.73m for UGent-1. The error of deleted ranging measurements were mostly concentrated at 2.0m and above. In multiple scenarios, the LS-SVM [24] algorithm combined with fixed CIR features and the CNN [35], CNN-LSTM [36] and Denoising Neural Network (D-NN) that is based on CNN, GRU and LSTM [37] algorithms combined with CIR raw sequences reduced the mean ranging measurement error by 21.19%, 35.17%, 54.35% and 57.49%, respectively.However, the proposed algorithm outperformed these methods, achieving reductions in mean ranging measurement error of 58.79%, 44.81%, 25.60%, and 22.49%, respectively. The LS-SVM algorithm has unstable performance due to the need to optimize feature composition according to different scenarios, with an average correction performance 58.80% lower than the algorithm proposed in this paper, and the highest being 61.84% in the LAB. CNN can self-extract measurement correction information from the CIR sequence, with an average correction performance

44.82% lower than the algorithm proposed in this paper. CNN focuses more on local spatial features, and combining it with LSTM, which is more suitable for sequential data, to form CNN-LSTM can further improve ranging measurement error correction performance, but it is still average 25.63% lower than the proposed algorithm. Compared to CNN-LSTM, D-NN introduces a GRU transition layer. The addition of GRU smooths the association between CNN-extracted local features and LSTM-derived long-term dependencies, enhancing the model's ability to capture the spatiotemporal characteristics of ranging errors in the CIR sequence. Nevertheless, the error correction performance of D-NN is, on average, 22.49% lower than that of the proposed algorithm, with a maximum difference of 31.09% observed in UGent-2. Overall, using CIR sequences alone yields better results than CIR feature vectors, but CNN, CNN-LSTM and D-NN cannot fuse the two effectively. This article proposes using BERT to simultaneously consider CIR features and CIR sequence correction for ranging errors, which can not only account for both temporal and energy information but also enable deep bidirectional learning to obtain more effective information. Additionally, the credibility evaluation proposed in this article can recall high-precision ranging measurements and discard worthless low-precision ones. Preventing high-precision ranging measurements from being incorrectly corrected and increasing, while also improving the accuracy of valuable correction data.

The time complexity of the proposed algorithm is $O(L(T^2 \cdot u + T \cdot u^2))$, where L represents the number of encoders, T denotes the input sequence length, and u is the embedding dimension. For LS-SVM, the time complexity is $O(n^2 \cdot m)$, where n is the number of samples, and m is the number of features. The time complexity of CNN is $O(L(W \cdot H \cdot F^2 \cdot D \cdot K))$, where $W \cdot H \cdot D$ represents the input dimensions (width, height, and depth), F is the filter size, K is the number of filters, and L is the number of convolutional layers. The complexity of CNN-LSTM increases by $O(T \cdot n^2)$ compared to CNN, where T is the sequence length, and n is the number of hidden units. Additionally, the complexity of D-NN increases by $O(T \cdot d_h \cdot (d_x + d_h))$ based on CNN-LSTM, where d_h is the dimension of the hidden state, and d_x is the input dimension. The algorithms were tested on a computer equipped with an Intel i7 processor and 16 GB of RAM. For three scenarios across four experimental campaigns, the testing data set size were 14,734, 15,298, 12,844, and 13,896 rows, respectively, summing to a total of 56,772 rows. On average, the proposed algorithm required 0.031 s per testing prediction, while the preduction time for LS-SVM, CNN, CNN-LSTM, and D-NN is 0.011 s, 0.017, 0.018 s, and 0.019 s, respectively.As shown, with a slightly higher computational timing cost, the proposed algorithm significantly improves range accuracy by 58. 8% while maintaining real-time operational capability that meets national requirements in real-time ranging computational timing of 0.1 s [38] .

Table 6
Horizontal comparison of NLOS ranging measurement error correction (m)

	LAB	CUMT	UGent-1	UGent-2
Original	1.400	1.093	1.457	1.232
Proposed	0.200	0.249	0.293	0.282
LS-SVM	1.066	0.776	1.190	1.065
CNN	0.770	0.565	1.169	0.893
CNN-LSTM	0.511	0.328	0.695	0.843
D-NN	0.486	0.452	0.583	0.665

5.3. Position

To verify the improvement in positioning accuracy achieved by the proposed credibility evaluation and ranging measurement error correction strategy, positioning experiments were conducted in three scenarios. The original positioning results were derived by combining the received UWB ranging data with the least squares positioning algorithm [26], using at least three LOS and NLOS measurements. Similarly, the corrected positioning results were obtained by applying the least squares positioning algorithm to high-confidence, corrected measurements. From Figure.8a, 8b and 8c, it is evident that the optimized positioning results do not contain significant large-scale offset data and more closely align with the preset trajectory. As shown in Figure.8d, except for the LAB scenario, the proportion of m-level positioning accuracy before and after optimization exceeds 99%. After optimization, the proportion of m-level positioning accuracy in the LAB scenario increased from 88.55% to 99.09%. The average percentage of cm-level positioning accuracy increased from 52.89% to 83.09%, with a maximum of 90.17% in the UGent scenario. As shown in Table.7, the Mean, Std, and RMSE of the optimized positioning error in multiple scenarios were reduced by 69.68%, 63.65%, and 59.08%, respectively, with the highest reductions being 75.69%, 74.43%, and 62.69%. Compared to advanced algorithms such as LS-SVM, CNN, CNN-LSTM and D-NN, our algorithm achieved an average lead of 26.89%, 22.61%, and 23.03% in the three indicators, with the maximum lead being 42.53%, 43.61%, and 44.00%. For three scenarios across four experimental sets, the data sizes were 970, 1,994, and 2,148 rows, respectively, totaling 5,112 rows. On average, the proposed algorithm required 0.055 s computational time per location, compared to 0.025 s, 0.042 s, 0.044 s, and 0.045 s by LS-SVM, CNN, CNN-LSTM, and D-NN, respectively. In particular, the proposed algorithms required only 0.055 s to identify, mitigate and calculate positioning results, while significantly improving positioning performance without compromising processing efficiency. The proposed algorithm has also met the national requirement in real-time positioning computational timing of 0.1s [38]

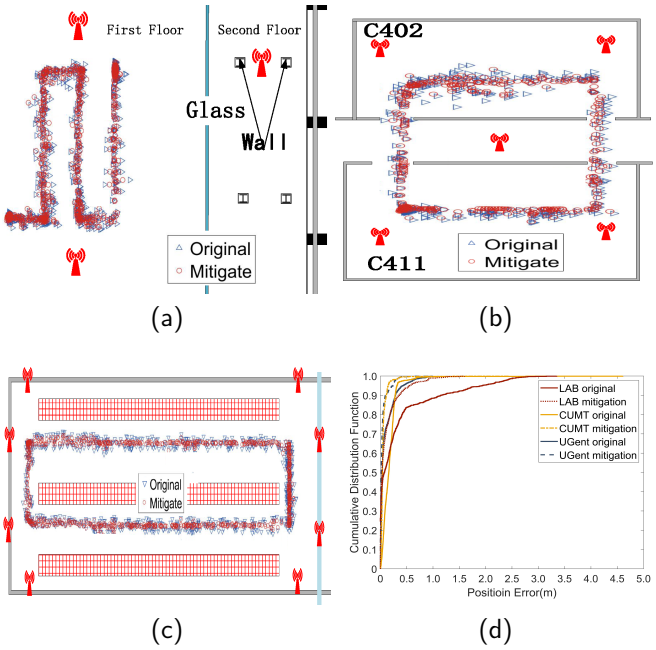

Figure 8: The Dynamic positioning trajectory before and after correction, (a) LAB, (b) CUMT,(c) UGent ,(d) CDF

Table 7
Dynamic positioning accuracy of different algorithms (m).

Scene	Algorithm	Mean	Std	Rmse
LAB	Original	0.251	0.222	0.150
	Proposed	0.061	0.092	0.067
	LS-SVM	0.159	0.154	0.113
	CNN	0.135	0.140	0.095
	CNN-LSTM	0.129	0.133	0.088
	D-NN	0.115	0.128	0.083
CUMT	Original	0.174	0.399	1.152
	Proposed	0.058	0.102	0.434
	LS-SVM	0.132	0.276	1.136
	CNN	0.109	0.210	0.860
	CNN-LSTM	0.082	0.187	0.755
	D-NN	0.091	0.179	0.139
UGent	Original	0.105	0.157	0.125
	Proposed	0.035	0.066	0.051
	LS-SVM	0.074	0.115	0.106
	CNN	0.067	0.097	0.083
	CNN-LSTM	0.051	0.084	0.069
	D-NN	0.054	0.087	0.075

6. Conclusion

To mitigate the impact of frequent indoor NLOS ranging measurement errors on UWB positioning accuracy, this paper develops a credibility evaluation model that assesses the quality of measurements using both simulated and empirical data. By analyzing waveforms associated with the causes of ranging errors, this paper performs a fine-grained classification of these errors. Based on the results of credibility evaluation and error classification, this paper prioritizes the retention of high-precision ranging measurements to fully leverage UWB technology, eliminates non-useful correction measurements, and constructs mitigation models to optimize valuable data. For different types of ranging measurement errors, BERT-LSTM correction models are developed to estimate both temporal and energy information simultaneously. Additionally, this approach is extended to LOS measurements. In the multi-scenario experiment, the Mean, Std, and RMSE of the credibility evaluation error were 0.047, 0.071, and 0.124, respectively. The ranging measurement error corresponding to the predicted credibility also meets the preset target. The average LOS ranging measurement error was reduced by 37.9%, with the proportion of m-level and cm-level accuracy increasing by 3.2% and 12.37%, respectively, reaching 98.53% and 58.07%. The average NLOS ranging measurement error was reduced by 80.94%, with the proportion of m-level accuracy increasing by 36.58% to 92.88%, and the maximum value of 90% ranging measurement error was reduced from 2.63m to 0.74m. Compared with advanced algorithms LS-SVM, CNN, and CNN-LSTM, our algorithm improved by 57.21%, 43.2%, and 18.99%, respectively. In terms of positioning accuracy, the optimized m-level positioning accuracy accounts for over 99%, while the cm-level positioning accuracy increased by 30.2% to 83.09%. The Mean, Std, and RMSE of optimized positioning errors were reduced by 69.68%, 63.65%, and 59.08%, respectively, with an average lead of 29.35%, 24.71%, and 25.41% over LS-SVM, CNN, and CNN-LSTM algorithms, and a maximum lead of 42.53%, 43.61%, and 44.00%.

References

[1] Mikoś, M., Kazmierski, K., Wachulec, N., Sośnica, K., 2024. Accuracy of satellite positioning using gnss receivers in sports watches. Measurement 229, 114426.

[2] Piao, W., Zhao, X., Li, Z., 2023. Mmgraphslam: Autonomous indoor positioning based on millimeter wave graphslam. Measurement 220, 113300.

[3] Fu, R., Xiao, D., Fan, Y., 2024. A novel cell phone localization solution for trapped victims based on compressed rssi fluctuation range and pso-bp neural network. Measurement 225, 114014.

[4] de Cerio, D.P.D., Ángela Hernández-Solana, Valdovinos, A., Olmos, J., Valenzuela, J.L., 2019. Low-cost test measurement setup for real iot ble sensor device characterization. Measurement 135, 814–827.

[5] Tian, Y., Lian, Z., Núñez-Andrés, M.A., Yue, Z., Li, K., Wang, P., Wang, M., 2024. The application of gated recurrent unit algorithm with fused attention mechanism in uwb indoor localization. Measurement 234, 114835.

[6] Wei, J., Su, S., Zhao, Z., Tong, X., Hu, L., Gao, W., 2023. Infrared pedestrian detection using improved unet and yolo through sharing visible light domain information. Measurement 221, 113442.

[7] Zheng, S., Li, Z., Yin, Y., Liu, Y., Zhang, H., Zheng, P., Zou, X., 2022. Multi-robot relative positioning and orientation system based on uwb range and graph optimization. Measurement 195, 111068.

[8] Venkatesh, S., Buehrer, R.M., 2007. Nlos mitigation using linear programming in ultrawideband location-aware networks. IEEE transactions on Vehicular Technology 56, 3182–3198.

[9] Chen, P.C., 1999. A non-line-of-sight error mitigation algorithm in location estimation, in: WCNC. 1999 IEEE wireless communications and networking conference (Cat. No. 99TH8466), pp. 316–320.

[10] Jiao, L., Xing, J., Zhang, X., Zhang, J., Zhao, C., 2007. Lcc-rwgh: A nlos error mitigation algorithm for localization in wireless

sensor network, in: 2007 IEEE international conference on control and automation, pp. 1354–1359.
[11] Bocus, M., Piechocki, R., Chetty, K., 2021. A comparison of uwb cir and wifi csi for human activity recognition, in: IEEE Radar Conference (RadarCon), p. 1.
[12] Liang, G., Gao, P., Li, L., Zhao, J., 2021. An indoor integrated localization algorithm based on uwb/ble, in: Journal of Physics: Conference Series, p. 012058.
[13] Álvarez-Merino, C.S., Luo-Chen, H.Q., Khatib, E.J., Barco, R., 2021. Wifi ftm, uwb and cellular-based radio fusion for indoor positioning. Sensors 21, 7020.
[14] Xia, J., Wang, Y., Jiang, B., Xiong, G., 2022. Research on indoor positioning system based on ble-aoa/uwb technology, in: 2022 41st Chinese Control Conference (CCC), pp. 5100–5105.
[15] Vandermeeren, S., Steendam, H., 2021. Pdr/uwb based positioning of a shopping cart. IEEE Sensors Journal 21, 10864–10878.
[16] Huang, Y., Mazuelas, S., Ge, F., Shen, Y., 2022. Indoor localization system with nlos mitigation based on self-training. IEEE Transactions on Mobile Computing 22, 3952–3966.
[17] Lin, H.Y., Zhan, J.R., 2023. Gnss-denied uav indoor navigation with uwb incorporated visual inertial odometry. Measurement 206, 112256.
[18] Heidari, M., Pahlavan, K., 2008. Identification of the absence of direct path in toa-based indoor localization systems. International Journal of Wireless Information Networks 15, 117–127.
[19] Dardari, D., Conti, A., Ferner, U., Giorgetti, A., Win, M.Z., 2009. Ranging with ultrawide bandwidth signals in multipath environments. Proceedings of the IEEE 97, 404–426.
[20] Chen, Y.Y., Huang, S.P., Wu, T.W., Tsai, W.T., Liou, C.Y., Mao, S.G., 2020. Uwb system for indoor positioning and tracking with arbitrary target orientation, optimal anchor location, and adaptive nlos mitigation. IEEE Transactions on Vehicular Technology 69, 9304–9314.
[21] Gao, Z., Jiao, Y., Yang, W., Li, X., Wang, Y., 2023. A method for uwb localization based on cnn-svm and hybrid locating algorithm. Information 14, 46.
[22] Gao, D., Zeng, X., Wang, J., Su, Y., 2020. Application of lstm network to improve indoor positioning accuracy. Sensors 20, 5824.
[23] Nkrow, R.E., Silva, B.J., Boshoff, D., Hancke, G.P., 2023. Uwb-based nlos identification and mitigation: A performance evaluation in dynamic settings, in: IECON 2023- 49th Annual Conference of the IEEE Industrial Electronics Society, pp. 1–6.
[24] Yu, K., Wen, K., Li, Y., Zhang, S., Zhang, K., 2018. A novel nlos mitigation algorithm for uwb localization in harsh indoor environments. IEEE Transactions on Vehicular Technology 68, 686–699.
[25] Marano, S., Gifford, W.M., Wymeersch, H., Win, M.Z., 2010. Nlos identification and mitigation for localization based on uwb experimental data. IEEE Journal on selected areas in communications 28, 1026–1035.
[26] Yang, H., Wang, Y., Seow, C.K., Sun, M., Si, M., Huang, L., 2023. Uwb sensor-based indoor los/nlos localization with support vector machine learning. IEEE Sensors Journal 23, 2988–3004.
[27] Kuhn, M.J., Turnmire, J., Mahfouz, M.R., Fathy, A.E., 2010. Adaptive leading-edge detection in uwb indoor localization, in: 2010 IEEE Radio and Wireless Symposium (RWS), pp. 268–271.
[28] Chen, Z., Chen, D., Zhang, X., Yuan, Z., Cheng, X., 2021. Learning graph structures with transformer for multivariate time-series anomaly detection in iot. IEEE Internet of Things Journal 9, 9179–9189.
[29] Vaswani, A., Shazeer, N., Parmar, N., Uszkoreit, J., Jones, L., Gomez, A., Polosukhin, I., 2017. Attention is all you need. paper presented at: Advances in neural information processing systems, in: 30 (nips 2017).
[30] Devlin, J., Chang, M.W., Lee, K., Toutanova, K., 2018. Bert: Pre-training of deep bidirectional transformers for language understanding. arXiv preprint arXiv:1810.04805 .
[31] Yang, H., Wang, Y., Seow, C., Sun, M., Plets, D., 2024. Uwb nlos identification and mitigation based on bidirectional encoder representations from transformer (bert) deep learning, in: 2024 14th International Conference on Indoor Positioning and Indoor Navigation (IPIN), pp. 1–6. doi:10.1109/IPIN62893.2024.10786116.
[32] Seow, C.K., Tan, S., 2008a. Localisation of mobile device in multi-path environment using bi-directional estimation. Electronics Letters 44, 1.
[33] Seow, C.K., Tan, S., 2008b. Non-line-of-sight unidirectional mobile localisation in multipath environment. Electronics Letters 44, 1.
[34] Ltd., D., 2015. Dw1000 user manual.
[35] Deng, B., Xu, T., Yan, M., 2023. Uwb nlos identification and mitigation based on gramian angular field and parallel deep learning model. IEEE Sensors Journal 23, 28513–28525. doi:10.1109/JSEN.2023.3323564.
[36] Tu, C., Zhang, J., Quan, Z., Ding, Y., 2024. Uwb indoor localization method based on neural network multi-classification for nlos distance correction. Sensors and Actuators A: Physical 379, 115904.
[37] Kim, D.H., Pyun, J.Y., 2024. Enhanced uwb ranging utilizing denoising neural network. IEEE Communications Letters 28, 1029–1033. doi:10.1109/LCOMM.2024.3374398.
[38] Zhu, J., Kang, Y., Zheng, Z., Lyu, M.R., 2012. Wsp: A network coordinate based web service positioning framework for response time prediction, in: 2012 IEEE 19th International Conference on Web Services, pp. 90–97. doi:10.1109/ICWS.2012.81.